ORIGINAL ARTICLE

Inducing mode analysis of rock burst in fault-affected zone with a hard–thick stratum occurrence

Pu Wang[1,2] · Li-shuai Jiang[3] · Peng-qiang Zheng[1,2] · Guang-peng Qin[1,2] · Chen Zhang[3]

Abstract

Study of movement characteristics of a hard–thick stratum (HTS) affected by a fault in a coalmine is significant to predict the dynamic hazards (i.e., rock bursts and shock bumps) because of the particular structural and mechanical properties of the HTS and the fault. Hence, using UDEC numerical simulation, the movement characteristic of HTS and fault-slipping law with different mining directions towards the fault were studied. Then, two different inducing modes and corresponding mechanisms of rock burst were obtained. The results show that the structure of overlying strata on two fault walls is different because of fault cutting and fault dip; it results in the HTS of two fault walls presenting different movement stage characteristics. From analysis of fault plane stress and fault slipping, we obtain that footwall mining has higher risk of rock burst than hanging wall mining. Finally, summarizing two different inducing modes of rock burst affected by the HTS and the fault: one that mainly resulted from the strain energy release caused by the HTS obvious bending and failure (i.e., hanging wall mining) and one that notably affected by fault slipping and HTS failure subsidence (i.e., footwall mining). A field case regarding microseismic monitoring is used to verify the numerical simulation results. Study results can serve as a reference for predicting of rock bursts and their classification into hazardous areas under similar conditions.

Keywords Hard–thick stratum (HTS) · Normal fault · Fault slipping · Rock burst

Introduction

With the increase of mining depth and mining stress for coal-mining activities, geological conditions are increasingly complex and the intensity of dynamic failure is more pronounced. This can result in more severe dynamic hazards, such as rock bursts, coal and gas outbursts, and shock bumps (Wang et al. 2016; Jiang et al. 2017; Wang et al. 2017; Jiang et al. 2018). Among these complex conditions, the fault and the hard–thick stratum (HTS) are the most common and representative triggers of dynamic failure (Wang et al. 2015; Jiang et al. 2019a, b).

According to statistical analysis of data for a large number of rock burst incidents, it indicates that the zone affected by geologic fault tectonics is more susceptible to dynamic disasters, because the displacement–stress field is affected by fault cutting and fault block (Qi and Dou 2008; Wang et al. 2018a, b, c). Moreover, from the structure characteristic of coal and rock masses in rock burst coalmines, it shows that a coal seam with bursting liability is common with a hard and thick stratum above it. This stratum will remain in suspension and compress the coal seam in the abutments, which will concentrate stress and accumulate a large store of strain energy. Hence, the rock burst can be easily induced once the large accumulation of strain energy releases suddenly (Lv et al. 2014; Wang et al. 2018a, b, c).

Hence, violent dynamic hazards are more easily caused with the common occurrence of a HTS and a fault and usually shown to be extreme destructive. For instance, a coal outburst accident occurred in the tailgate of panel 6303, Jining coalmine in 2004 because of the coupling effect of a

✉ Peng-qiang Zheng
pqzheng_1231@163.com

1 Department of Resources and Civil Engineering, Shandong University of Science and Technology, Tai'an 271019, China

2 National Engineering Laboratory for Coalmine Backfilling Mining, Shandong University of Science and Technology, Tai'an 271019, China

3 State Key Laboratory of Mining Disaster Prevention and Control Co–Founded by Shandong Province and the Ministry of Science and Technology, Shandong University of Science and Technology, Qingdao 266590, China

medium sandstone (thickness: 20 m) and a fault marked as SF28. A shock bump with many casualties occurred in the tailgate of panel 2310, Baodian coalmine in 2004, which was affected by a medium sandstone (thickness of 94.27 m) and the Damachang fault (vertical displacement of 10 m). A rock burst accident with roadway instability and fatalities occurred in Muchengjian coalmine in 2005 due to the effect of main roof with pack sand (thickness: 94.27 m) and two faults of F3-1 and F 3-2. These accidents caused very serious disasters, such as coal outburst, rock burst, shock bump, serious roadway damage, and fatalities. Figure 1 shows several images captured on-site after the accidents.

Considerable studies have been conducted using different methods with regard to the occurrence of an HTS or a fault. For instance, Ning et al. (2017), Wang et al. (2015, 2016), and Zhao et al. (2017) used theoretical analysis, similar simulation test, and field observation to analyze the initial breaking and migration of the HTS in detail; and then, the methods of roof control for the HTS, such as long-hole presplit blasting and hydraulic presplitting, were put forward. Xia et al. (2017) studied the influence of remaining coal pillars on hard stratum fractures, as well as mine pressure behaviors under their coupling effects by utilizing theoretical analysis, similar experiments, numerical simulations, and field tests. Wang et al. (2013) studied the controlling effects of a thick, hard igneous rock on pressure-relief gas drainage, and coal seam outbursts using the physical simulation test; moreover, some control measures were put forward. Ji et al. (2012) studied the stress evolution of a working face in footwall: one that was parallel to and one that was perpendicular to a fault. Cao et al. (2001) investigated four coalmines in Pingdingshan coal field (China) in detail and determined that coal and gas outbursts with reverse faults nearly always occurred in the footwalls. Sainoki and Mitri (2014a) used the dynamic numerical analysis to study and reveal the fault-slipping mechanism; results showed that fault dip angle and mining depth affected the fault slipping, whereas the effects of fault stiffness and dilation angle were negligible. Sainoki and Mitri (2014b, 2015b) incorporated Barton's shear-strength model into the FLAC3D numerical modeling code to study the potential effect of a fault-slip burst on mine openings; moreover, the model revealed that faults with rough surfaces tend to cause much larger seismic

events than do those with smooth surfaces. Zhou et al. (2015) studied the induced mechanism of rock bursts caused by a small-scale structural plane for which three types of rock bursts were classified. Jiang et al. (2015) and Zhao and Lv (2015) studied the stress distributions to understand the coupling effect of a thick hard roof and a reverse fault; then, revealed the rock burst mechanism and controlling methods. Wang et al. (2018a, b, c) studied the strata behaviors and rock burst-inducing mechanism using the universal distinct element code numerical simulation when the working face passed through the fault; moreover, the mechanism that induces rock bursts can be divided into two stages.

Most of the previous studies have been carried out on mining stress distribution and rock response of either the HTS or fault only; however, the coupling effect of the HTS and the fault on rock bursts was rarely discussed. Hence, in this study, a numerical model related to the relative position between the HTS (thickness: 60 m) and a normal fault (dip angle: 60°) is established using the UDEC simulation software. Then, the movement characteristic of HTS and fault displacement in fault-affected zone are studied with different mining directions. Subsequently, two different inducing modes and corresponding mechanisms of rock burst were obtained. The study results can provide a technical basis for research on rock bursts, coal and gas outbursts, and roof control of mining pressure under similar conditions (Rutqvist et al. 2015; Li et al. 2016).

UDEC numerical model establishment

As described in previous section, to highlight the purpose and effect of this study, the thickness of HTS is set to 60 m, and the distance between the HTS and coal seam is also 60 m. Hence, considering the boundary effect, a numerical model of 700 m (length) × 238 m (height) was established, as shown in Fig. 2. The model is divided into three parts (i.e., a hanging wall, a footwall, and a fault zone) and built separately (Sainoki and Mitri 2015a; Jiang et al. 2016). In the minewide model, meshes are discretized more densely around coal seam where the stopes were extracted compared to the meshes in the areas near the model boundary. Thus, the immediate roof splits into random joints to obtain more

Fig. 1 Images captured on-site after accidents (Wang et al. 2018a, b, c)
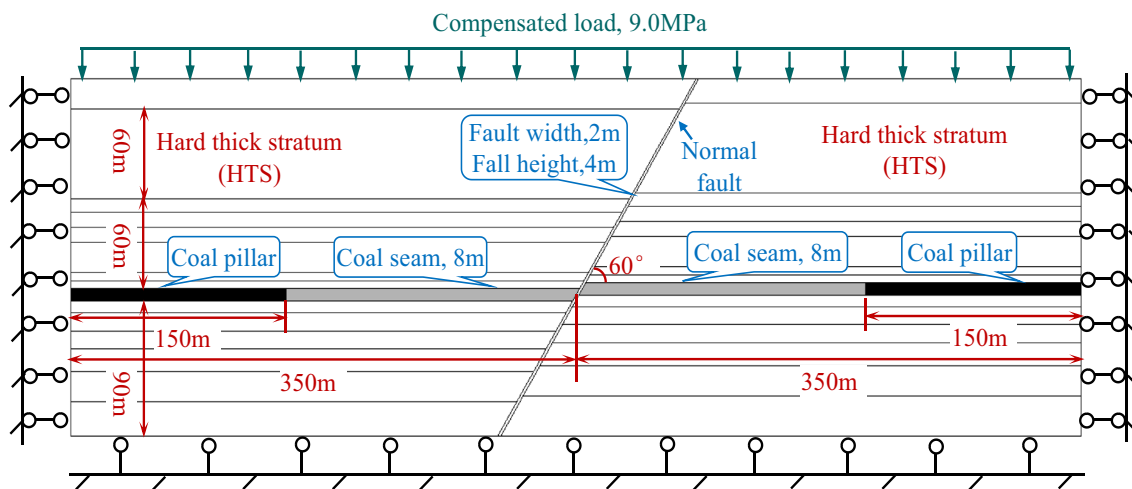
Fig. 2 Numerical calculation model

realistic results (Sainoki and Mitri 2014c, 2015a; Hofmann and Scheepers 2015; Jiang et al. 2017; Jiang et al. 2019a, b). In this model, the main characteristics are as follows: the thickness of coal seam is 8 m, mining depth is set at 500 m, fault dip angle is 60°, fault vertical displacement is 4 m, and broken-belt width of fault is 2 m.

As to the mechanical properties of the blocks and joints applied to the model, they usually derived from laboratory testing (Sainoki and Mitri 2015a; Alshkane et al. 2017). As shown in Table 1, the parameters of rock masses and fault which derived from previous studies are listed (Jiang et al. 2015; Sainoki and Mitri 2015a; Barton and Choubey 1977). The Mohr–Coulomb model is used to simulate the continuous part of rocks and the joint-surface contact-Coulomb slip model is used to simulate the joint calculation (Itasca Consulting Group 2005). For the Mohr–Coulomb failure criterion, a zero-cohesion and zero-tension are assumed, because the cohesive strength of a fault or joint is generally quite low (Sainoki and Mitri 2014c).

The bottom of model is set up with a full-displacement constraint, the sides of model (i.e., left side and right side of model) use a horizontal displacement constraint and vertical displacement free boundary, and the top boundary is viewed as free. Moreover, the compensated load should be applied on the top of model to simulate the failed simulation depth of on-site model, and are calculated by $\sigma = \gamma h = 25 \text{ kN m}^{-3} \times 360 \text{ m} = 9.0 \text{ MPa}$, where σ is the compensated load, γ is the unit weight of failed simulated rocks, and h is the height of failed simulated strata, in this study, h is 360 m.

Movement characteristics of overlying strata

Two displacement-monitoring lines marked as D1 and SD1 are laid out, as shown in Fig. 3, to monitor the subsidence of HTS and the strata under the HTS. D1 locates in the strata under HTS with vertical distance of 55 m from the footwall coal seam; while SD1 is in the HTS with vertical distance of 65 m from the hanging wall coal seam.

Hanging wall mining

When the working face originates in hanging wall, and extraction towards the fault, some diagrams of strata

Table 1 Mechanical properties of rock masses

Lithology	Density/kg m^{-3}	Bulk/GPa	Shear/GPa	Cohesive/MPa	Tensile strength/MPa	Internal friction angle/°
Siltstone	2530	8.82	4.84	3.30	2.47	30
Pack sand	2530	13.4	7.60	3.26	2.19	28
Gritstone	2540	6.87	3.3	3.16	2.19	28
Mudstone	2340	2.17	1.00	1.30	1.15	38
Coal	1350	2.35	1.47	1.10	1.50	20
Fault	2000	1.78	1.28	0	0	30
HTS	3000	75	47	15	25	45

**Fig. 3** Layout of stress/displacement-monitoring lines or points
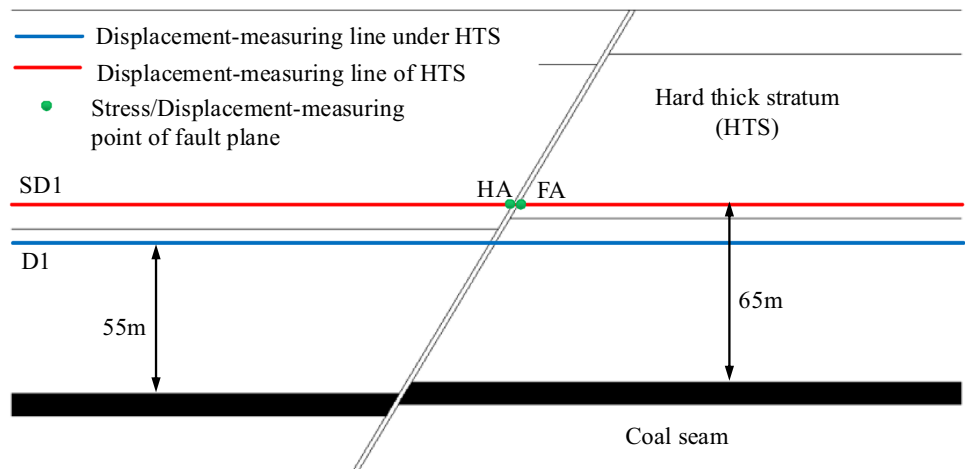
movement with face mining are selected, as shown in Fig. 4. Figure 5 depicts the curves of subsidence variation of HTS and the underlying stratum reflected by D1 and SD1.

In Fig. 5, when the distance between the working face and fault exceeds 90 m, which is defined as $L_h > 90$ m, the strata under the HTS moves and continuously develops upwards; then, the maximum subsidence value of D1 increases gradually and rises to 0.61 m with $L_h = 100$ m. However, because of the support provided by the underlying strata, the HTS subsidence is limited and does not change rapidly.

When $L_h = 90$ m, the strata under HTS moves together with inferior key stratum breaking and movement, and then, the notable bed separation is observed under HTS, as shown in Fig. 4a. Hence, the subsidence values of D1 increase significantly and the maximum value sharply rises to 3.76 m. Meanwhile, because of high stiffness and strength of HTS, its deformation remains small, and arching within the stiffer HTS results in "suspension" above the area of bed separation.

When 90 m > $L_h \geq 30$ m, the inferior key stratum and its surrounding rocks move and subside further with the goaf

(a)

(b)

(c)

(d)
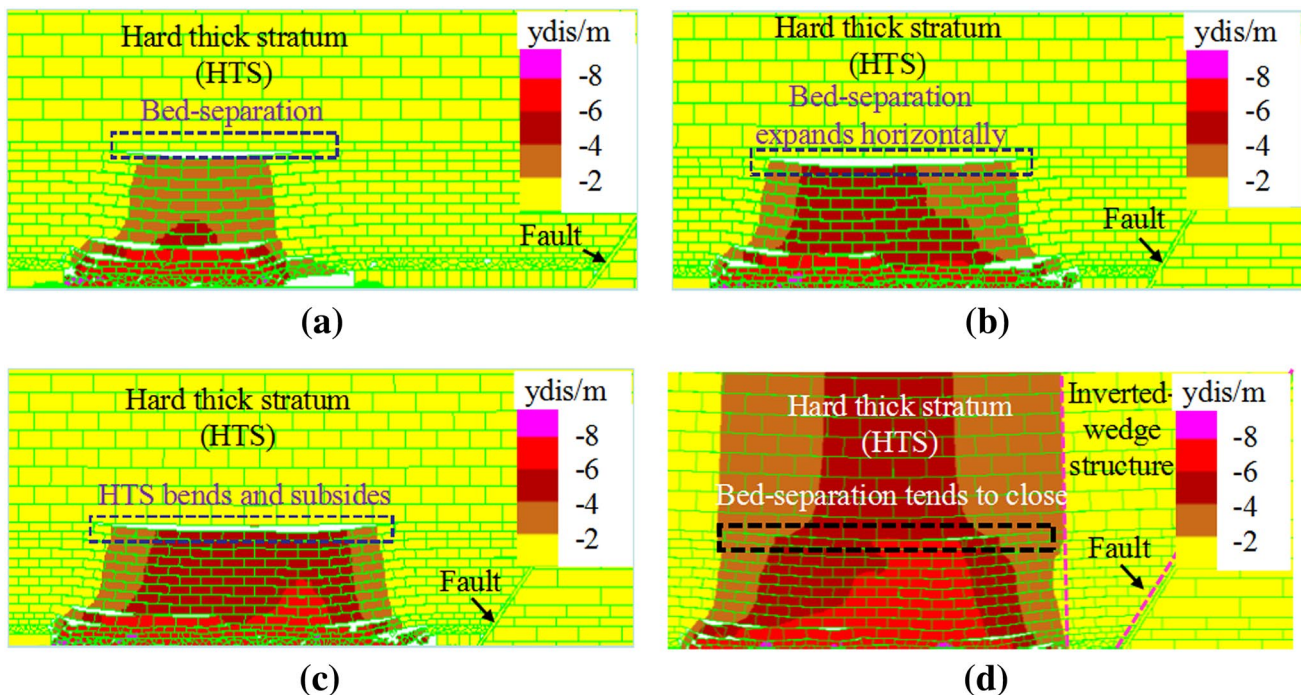
Fig. 4 Diagrams of strata movement with hanging wall mining: **a** bed separation develops to the bottom of HTS with $L_h = 90$ m; **b** bed separation expands horizontally with $L_h = 30$ m; **c** HTS bends and subsides with $L_h = 20$ m; **d** HTS subsides notably and bed separation tends to close with $L_h = 10$ m
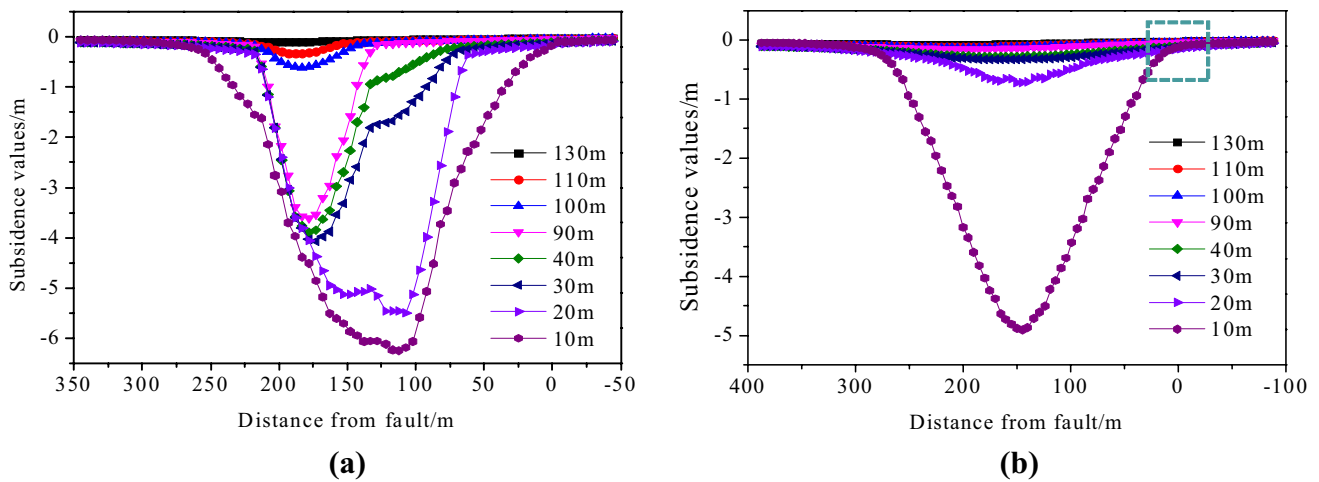
Fig. 5 Curves of subsidence variation of HTS and underlying stratum with hanging wall mining: **a** measuring line D1; **b** measuring line SD1

expanding, and hence, the maximum values of D1 increase gradually. The subsidence value of HTS is still small. However, the HTS blocks the upwards development of bed separation and only shows obvious lateral expansion, as shown in Fig. 4b.

When $L_h = 20$ m, with the periodic breaking and movement of inferior key stratum, the subsidence range under the HTS extends notably. Hence, the maximum subsidence value of D1 significantly increases to 5.5 m and moves forward. However, the HTS experiences bending and subsidence, and the maximum subsidence value is 0.72 m. Moreover, the bed separation under HTS continues to expand horizontally, as shown in Fig. 4c.

When $L_h = 10$ m, with the ongoing movement of the strata under HTS and the caved rocks compaction, the subsidence

values of D1 increase slightly. However, the HTS subsides notably due to the undercut span exceeding its ultimate stable length (as shown in Fig. 4d), and the maximum subsidence value sharply rises to 4.87 m.

Thus, when the working face mines in hanging wall towards the fault, an inverted-wedge structure of overlying strata in hanging wall which has a good stability is formed affected by the fault cutting. It indicates that the movement of overlying strata is not obviously affected by the fault, but influenced significantly by HTS movement. Figure 6 shows the variation curves of HTS displacement in the vicinity of fault, which is deduced from the local enlarged drawing of Fig. 5b with dotted box. We can see that when $L_h = 10$ m, the HTS of two fault walls has certain displacement which indicates that even though the effect of fault on the movement of

(a) Vertical displacement   **(b)** Horizontal displacement
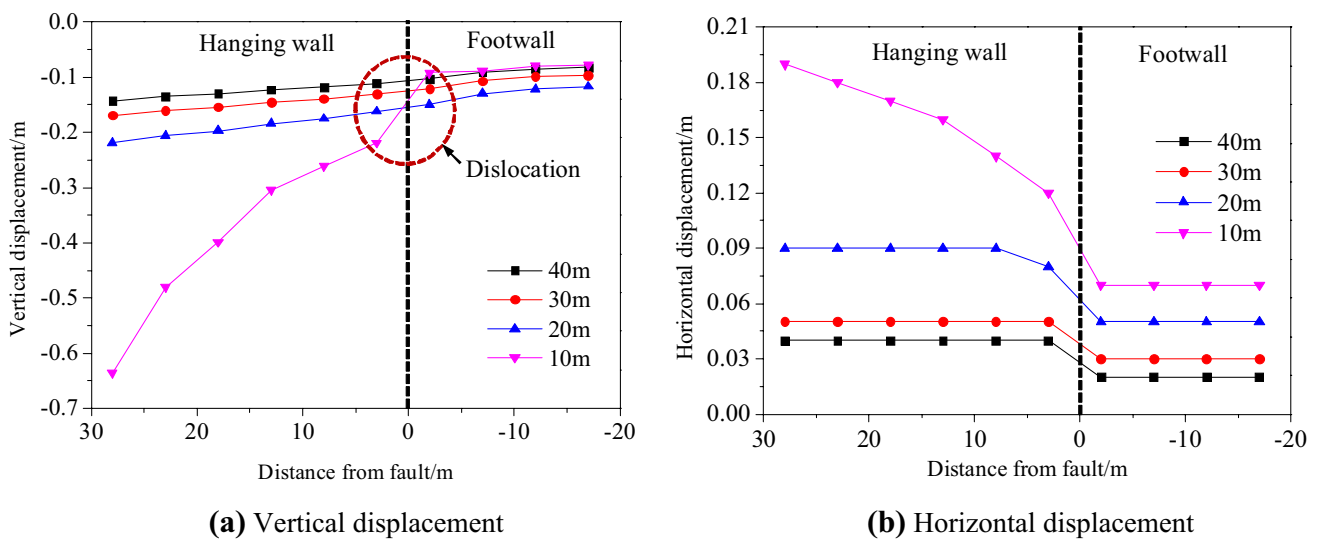
Fig. 6 Curves of HTS movement near the fault with hanging wall mining

overlying strata is not obvious, the HTS movement near the fault is still affected by the fault.
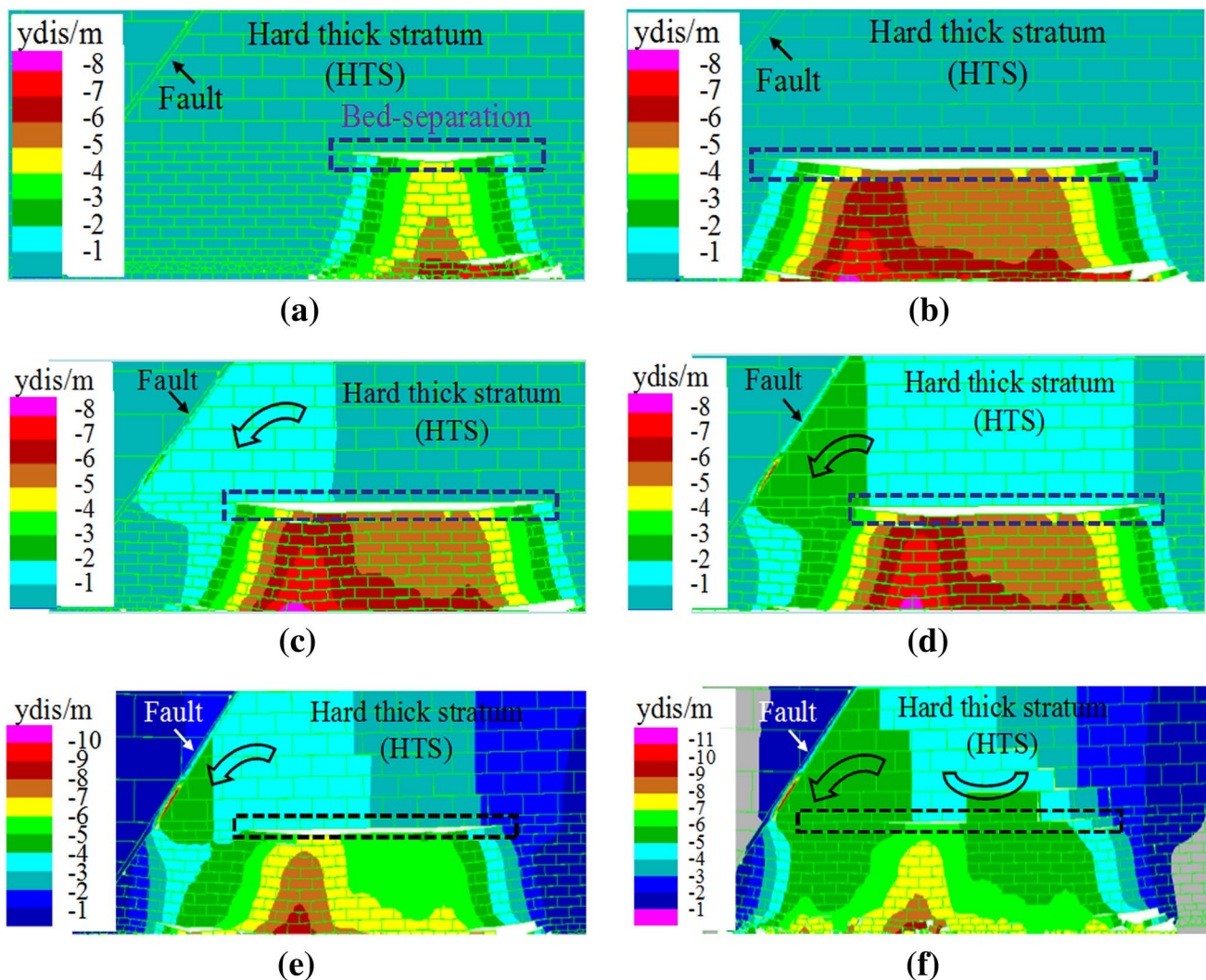
Footwall mining

Figures 7, 8 depict the diagrams of strata movement and subsidence variations of the HTS and its underlying strata when a working face advances in the footwall towards the fault.

When a working face in a footwall advances towards the fault, we define the distance between the working face and the fault as L_f. When $L_f \geq 50$ m, as shown in Figs. 7a, b, the strata under HTS move and continuously deform upwards; moreover, the bed separation occurs under HTS and continues to exhibit lateral expansion. The movement characteristic of overlying strata is same as that of hanging wall mining.

Hence, the subsidence of overlying strata is not affected by fault which is also same with the hanging wall mining, as shown in Fig. 8a. However, when $L_f = 50$ m, the bearing capacity of lower strata to HTS reduces due to fault cutting and fault dip, which results in a small displacement of SD1 caused by HTS rotating towards fault. Hence, a displacement discrepancy occurs between the two fault surfaces, as shown in Fig. 8b.

When 50 m $> L_f \geq 30$ m, the range of mining disturbance in overlying strata under HTS increases which leads to the increase in subsidence values of D1. However, because of the bearing capacity of lower strata to HTS reducing further, the HTS rotates towards the fault and slips along the fault, as shown in Fig. 7c, d. It indicates that overlying strata movement is affected by fault and gradually intensifies.

Fig. 7 Diagrams of strata movement with footwall mining: **a** bed separation develops to the bottom of HTS with $L_f = 110$ m; **b** bed separation expands horizontally with $L_f = 50$ m; **c** bed separation continues to expand and HTS rotates towards fault with $L_f = 40$ m; **d** bed separation decreases and HTS notable rotation towards fault $L_f = 30$ m; **e** HTS rotation towards fault increased with $L_f = 20$ m; **f** bed separation tends to close, HTS subsides and slips notably with $L_f = 10$ m
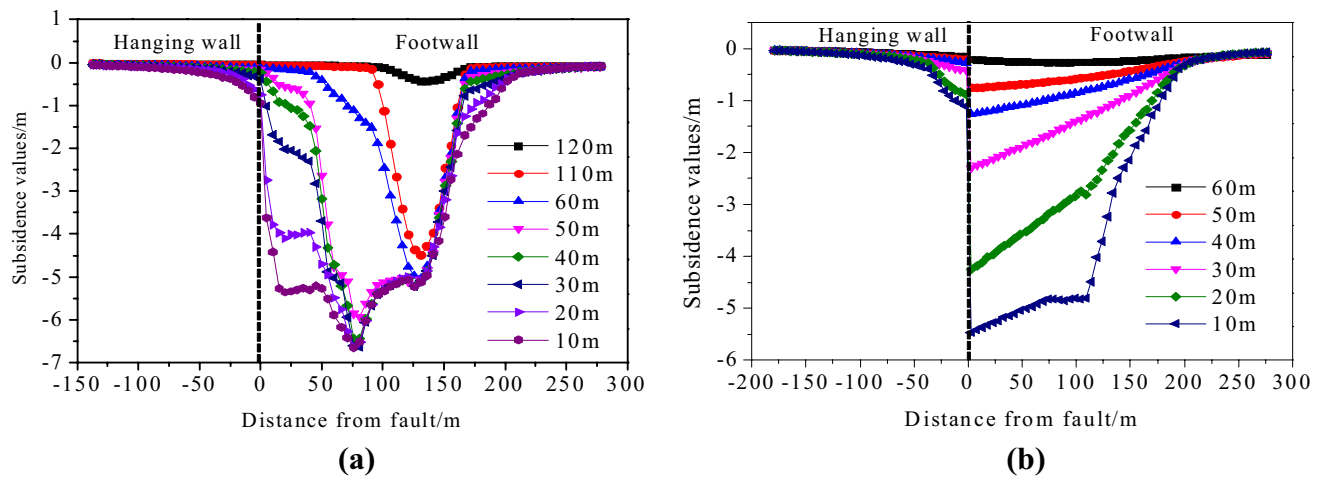
Fig. 8 Curves of subsidence variation of HTS and its underlying strata with footwall mining: **a** measuring line D1; **b** measuring line SD1

When 30 m > L_f ≥ 10 m, in Fig. 7e, f, the strata under HTS is affected by the fault obviously and a displacement mutation occurs. Meanwhile, the bearing capacity of lower strata to HTS reduces notably which aggravates HTS rotation towards the fault, and hence, the subsidence of SD1 increases sharply and the maximum value rises to 5.46 m with L_f = 10 m. Then, the HTS bends and breaks, thereby resulting in the bed separation under HTS tending to close gradually. It indicates that the overlying strata movement is affected by fault notably; moreover, the final displacement of the HTS is caused by the rotation slipping and bending subsidence of HTS, and the former contributes much more. In addition, because of the large range movement of footwall strata, the HTS in hanging wall also occurs obvious rotation and subsidence, but the displacement dislocation of two fault walls increases significantly, as shown in Fig. 8b.

When the working face in footwall mines towards the fault, the bearing capacity of lower strata to HTS reduces notably which leads to the HTS easily rotating towards the fault and slipping along the fault; and then, the HTS bends and breaks, it occurs a notable displacement. The final displacement is caused by the rotation slipping and bending subsidence of HTS, and the former contributes much more.

Thus, under the coupling effect of an HTS and a fault, an inverted-wedge structure in hanging wall has a good stability because of the fault cutting and fault dip; hence, the final displacement of HTS with hanging wall mining is mainly affected by its bending and subsidence. However, the final displacement of HTS with footwall mining is caused by its rotation slipping and bending subsidence, and the former contributes much more. In addition, we can also conclude that the influence of the fault with footwall mining is more significant than that of hanging wall mining.

## Analysis of fault activation and slipping

Analysis of fault plane stress caused by mining

Two stress-monitoring points, marked as HA (in hanging wall) and FA (in footwall) in Fig. 3, were selected on the interface between HTS and fault plane from SD1 to monitor the fault plane stress. The normal stress and shear stress of eight mining states, which correspond to distances of 80–10 m with interval of 10 m between the working face and the fault, are displayed, and then, the ratio of the shear stress to the normal stress was calculated. The curves of shear stress, normal stress, and the ratio of the shear stress to the normal stress of the two measuring points with different mining directions are shown in Fig. 9.

From Fig. 9c, we can seen that for either footwall mining or hanging wall mining, the ratio of shear stress to normal stress of fault plane has obvious spatiotemporal characteristics. When the distance from the fault is larger, the ratio is small and increases gradually as the distance is reduced; whereas, it increases sharply and remains a high level when the face is closer to the fault. However, the variations of shear stress and normal stress of fault plane with different mining directions still have great differences, as shown in Fig. 9a, b.

When 80 m ≥ L_h ≥ 20 m, when mining from the hanging wall towards the fault, the inverted-wedge structure of overlying strata defined by the fault shows gradual increasing of shear stress and normal stress; the ratio is small, but is basically linear growth. It indicates that the effect of mining disturbance on fault is small, thereby increasing the possibility of fault activation gradually.

When 80 m ≥ L_f ≥ 30 m, with the mining front advancing from the footwall, the fault bonding capacity at the HTS decreases which leads to normal stress drops and shear stress

**(a)**

(b)

(c)
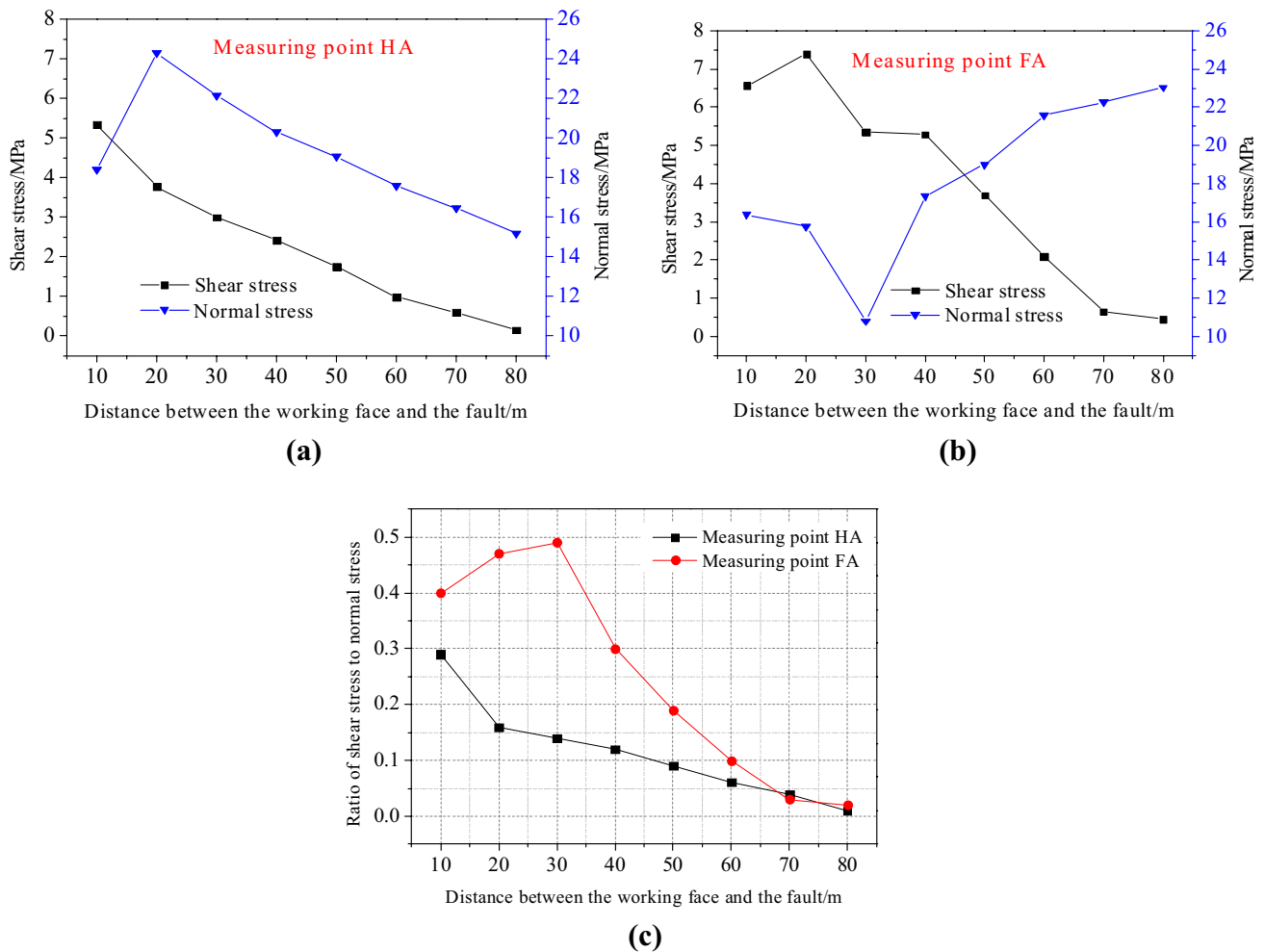
Fig. 9 Curves of fault plane stress and its ratio with different mining sequence: **a** measuring point HA with hanging wall mining; **b** measuring point FA with footwall mining; **c** ratio of shear stress to normal stress with different mining sequence

rises. The normal stress and shear stress are 10.80 MPa and 5.34 MPa with $L_f = 30$ m, and the ratio of shear stress to normal stress increases notably to 0.49 which indicates the possibility of fault activation. When 30 m $> L_f \geq 10$ m, because of footwall HTS notable rotation and subsidence, the hanging wall HTS also rotates and extrudes the footwall. Hence, both the normal stress and shear stress rise but at different rates, which results in a slight decrease in the ratio of shear to normal stress, but still has a large value. It shows that the possibility of fault activation is still high.

Analysis of fault slipping caused by mining

Figure 10 depicts the relative subsidence values of two fault walls, which can represent the fault slipping values. When $L_f \geq 50$ m and $L_h \geq 50$ m, the slipping values of fault at HTS basically tend to zero, which indicates that fault and its dip have little effect on the fault slipping. However, the effect of
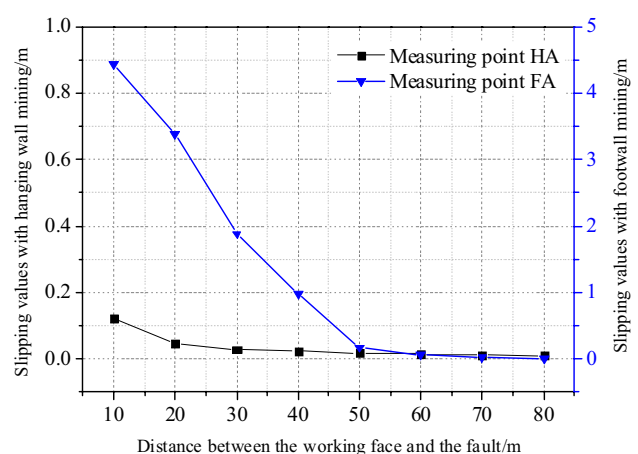
Fig. 10 Variation curves of fault slipping

fault dip on fault slipping at HTS is obviously different with $50 > L_f \geq 10$ m and $50 > L_h \geq 10$ m.

When $L_h < 50$ m, although the fault slipping value rises, it is at a low level overall. The slipping rate (reflect by curve slope) is larger only at the distance from the fault 10 m, which is significantly increased from 0.047 to 0.122 m. At this time, it is exactly the stage of notable subsidence for the HTS, so the fault slipping may be caused by HTS movement. However, when $L_f < 50$ m, the fault slipping values are significant and increase sharply, and the maximum value rises to 4.44 m with $L_f = 10$ m. It indicates that the fault is strongly affected by mining disturbance; moreover, the fault band and elastic rock system may be in a state of instability, resulting in significant dislocation of two fault walls, which is easy to induce fault-slip rock burst.

From Figs. 9 and 10, it can be seen that the stress ratio and fault-slip values are greater with footwall mining than that caused by mining from the hanging wall: for instance, the maximum slipping value during hanging wall mining only accounts for 2.75% that of the footwall mining. It indicates that the risk of fault-slip rock bursts during footwall mining is larger than that during hanging wall mining.

Inducing modes and mechanisms of rock burst

According to the analysis, two different triggers of rock burst can occur with different mining direction due to the change in the deformation and stress induced in the rock mass adjacent to the fault.

When the hanging wall face advances towards the fault, a high abutment stress concentrates and a large amount of strain energy accumulates in the shrinking pillar between the fault and the coal face, which has potential hazards with strain burst. With the HTS subsidence and failure, the concentrated stress in hanging wall drops and a large amount of strain energy is released which will easily induce a strain burst; meanwhile, the strain energy released by HTS subsidence helps the fault activate and slip, and can continue to release energy, thereby inducing the fault-slip rock burst. Figure 11 shows the inducing mode and mechanism of rock burst during hanging wall mining.

When the footwall face advances towards the fault, the suspended HTS rotates towards the fault and slips along the fault due to undercutting and reduction in confining stresses due to settlement of the HTS. The fault actives violently and the fault band and elastic rock system lose stability which results in a large amount of energy releasing. Meanwhile, a part of energy will release with HTS failure and movement; however, the HTS after failure continues to slip along the fault and release energy sequentially. Hence, a more severe rock burst can be induced if the two different sources of energy release occur concurrently, or in superposition. Figure 12 shows the inducing mode and mechanism of rock burst during hanging wall mining.

Engineering case

In this section, according to the field observation data of microseismic activity monitored by seismological observation system (SOS), which is developed by the Poland Central Mining Institute and widely used to monitor dynamic rock mass failures in coalmines (Xu et al. 2011), during mining operation of panel $103_{down}03$ in Baodian coalmine, the relationship among the advance of the mining operation, fault activation, and microseismic activities is analyzed to further verify the previous results of numerical simulation.

Geological conditions

Figure 13 shows the position of the panel $103_{down}03$. The panel $103_{down}03$ has 521 m mining depth. The average thickness of coal seam is 3.26 m and its average dip angle is 8°. The hardness coefficient of coal seam is 3.1, which indicates that it has strong bursting potential. According to the borehole histogram, the lithologies of rock masses are
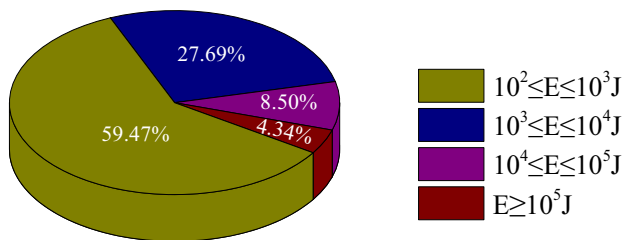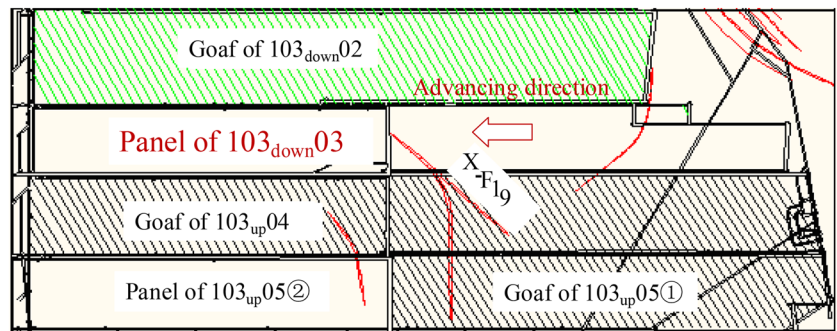

Fig. 11 Mode of rock burst during hanging wall mining
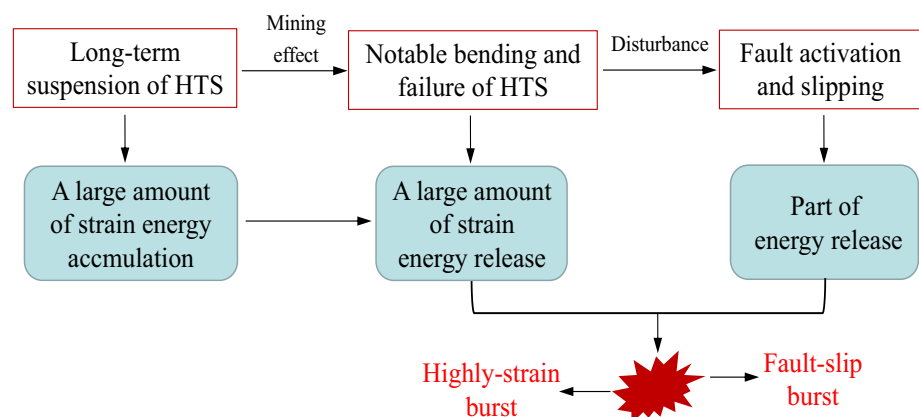
Fig. 12 Mode of rock burst during footwall mining
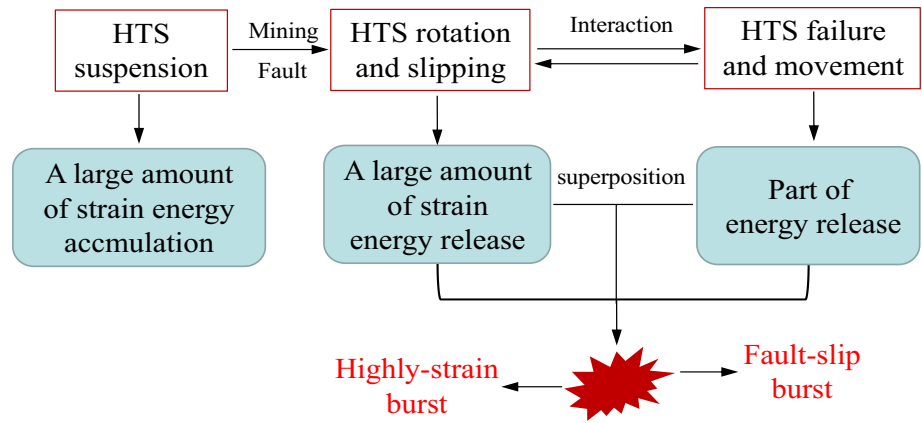
Fig. 13 Plan of panel of $103_{down}03$ (Jiang et al. 2017)

Fig. 14 Proportions of microseismic events at different energy levels

mainly sandstone and a thick-and-hard medium-fine sandstone stratum with a thickness of 156.86 m occurs and the vertical distance from the coal seam is 187.46 m. Based on the field report, a normal fault (marked as X-F19) located in the middle of working face has notable effect on its mining.
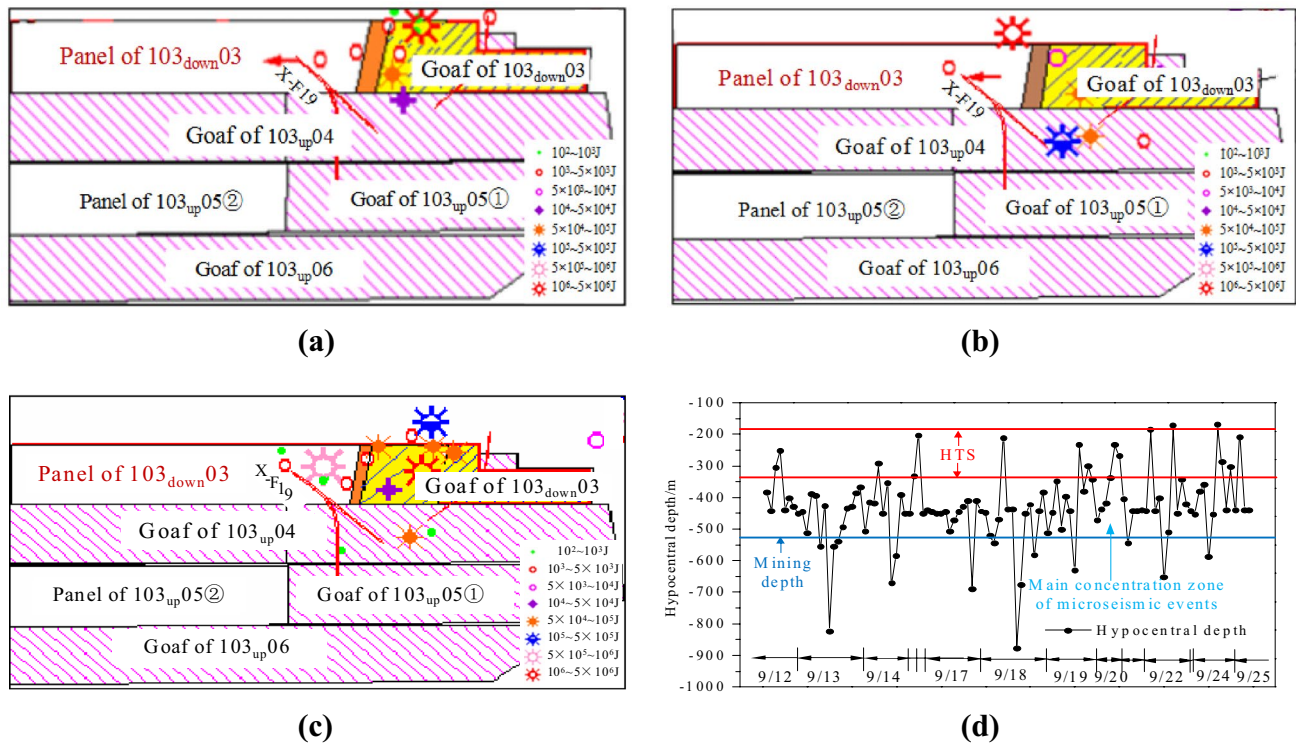
Microseismic events and its analysis

The mining of panel $103_{down}03$ commenced on June 12, 2011 and completed on 15 March, 2012. During the mining of panel $103_{down}03$, a total of 2672 microseismic events were monitored, and the number of microseismic events with $E \geq 10^5$ J was 116 which accounted for 4.34% of all events, as shown in Fig. 14. It indicates that microseismic events are mainly small energy events, and they have little effect on

mine safety; however, even though the microseismic events with $E \geq 10^5$ J are less frequency, they have great influence on the mining space and surface due to the large energy release. For instance, a strong shock bump with large energy of 535,142.1 J occurred near the fault of X-F19 in September 29, 2011 and the vibration was notable in the working face.

The microseismic events monitored when panel $103_{down}03$ in footwall approaches X-F19 during September 12, 2011 to October 2, 2011, which are chosen to study the spatial–temporal distributions of microseismic activities with common occurrence of an HTS and a fault, as shown in Fig. 15. From Figs. 15a, b, and d, it can be seen that microseismic activities are mainly distributed in the goaf of working face and the HTS underlying strata. This is because the strata under HTS are disturbed and failure affected by mining operation, so many microseismic events with small energy are formed. In addition, because of the HTS stability affected by mining, several microseismic events with large energy exceeding 10^5 J were also induced, and hence, monitoring and prevention should be also strengthened at this stage.

In Fig. 15c, the panel $103_{down}03$ mined during September 26, 2011–October 2, 2011, the number of microseismic events between the working face and the fault X-F19 increased notably, as did the amount of energy released. A microseismic event with a release of energy

Fig. 15 Planar distribution of microseismic events (2011.9.12~10.2) and its hypocentral depth (2011.9.12~9.25) (Jiang et al. 2017): **a** 2011.9.12~9/18; **b** 2011.9.19~9.25; **c** 2011.9.26~10.2; **d** hypocentral depth of microseismic events
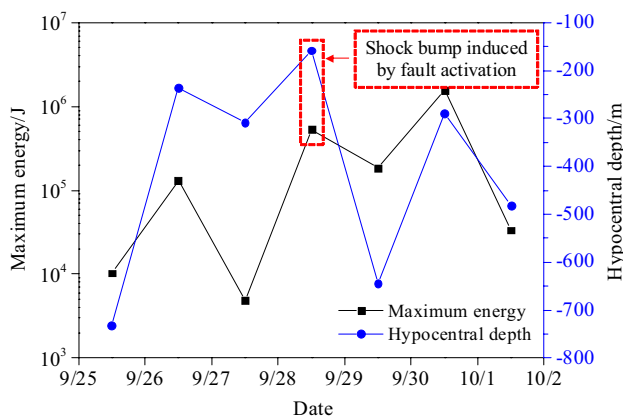
Fig. 16 Maximum energy and hypocentral depth of microseismic events (2011.9.26~10.2) (Jiang et al. 2017)

greater than 10^5 J occurred in the vicinity of fault. Figure 16 is the maximum energy and its hypocentral depth of microseismic activities when panel $103_{down}03$ in footwall approaches fault X-F19. It can be seen that the number of microseismic events is more intensive due to a presence of the fault and the maximum energy level of microseismic events is relatively high. A strong shock bump with large energy of 535,142.1 J occurred near fault X-F19 in September 29, 2011 was monitored and the hypocentral depth is about -158.08 m which is just in the HTS above the goaf. The suspected cause based on field data is that mining activities induce the largely suspended HTS to fail and activate the fault which results in releasing of a large amount of strain energy, thereby inducing this strong shock bump. Hence, the field observation can verify the aforementioned results of numerical simulation, that is the common occurrence of a HTS and a fault may induce more severe dynamic events due to HTS large-scale suspension and fault activation slipping.

Conclusions

In this study, the inducing characteristics analysis of rock burst in fault-affected zone with a hard–thick stratum occurrence was analyzed. Moreover, two different inducing modes and mechanism of rock burst were studied using UDEC numerical simulation and field observation. We can obtain several conclusions as follows.

- The structure of overlying strata on two fault walls is different because of fault cutting and fault dip; it results in the HTS on two fault walls presenting different movement stage characteristics.

- From analysis of fault plane stress and fault slipping, footwall mining has higher risk of rock burst than hanging wall mining.
- Summarizing two different modes of rock burst affected by the HTS and the fault: one that mainly resulted from the strain energy release caused by the HTS bending and failure (i.e., hanging wall mining) and one that notably is affected by fault slipping and HTS failure subsidence (i.e., footwall mining).

Finally, a field case regarding microseismic monitoring is used to verify the numerical simulation results.

The study results can serve as a reference for predicting of rock bursts and their classification into hazardous areas under similar conditions.

References

Alshkane YM, Marshall AM, Stace LR (2017) Prediction of strength and deformability of an interlocked blocky rock mass using UDEC. J Rock Mech Geotech Eng 9(3):531–542

Barton N, Choubey V (1977) The shear strength of rock joints in theory and practice. Rock Mech 10:1–54

Cao YX, He DD, Glick DC (2001) Coal and gas outbursts in footwalls of reverse faults. Int J Coal Geol 48(1–2):47–63

Hofmann GF, Scheepers LJ (2015) Simulating fault slip areas of mining induced seismic tremors using static boundary element numerical modeling. Trans Inst Min Metal 120(1):53–64

Itasca (2005) Universal distinct element code user's guide (Version 4.0). Itasca Consulting Group, Minneapolis, USA

Ji HG, Ma HS, Wang JA, Zhang YH, Cao H (2012) Mining disturbance effect and mining arrangements analysis of near-fault mining in high tectonic stress region. Saf Sci 50(4):649–654

Jiang JQ, Wu QL, Qu H (2015) Characteristic of mining stress evolution and activation of the reverse fault below the hard-thick strata. J China Coal Soc 40(2):267–277 **(Chinese)**

Jiang LS, Sainoki A, Mitri HS, Ma NJ, Liu HT, Hao Z (2016) Influence of fracture-induced weakening on coal mine gateroad stability. Int J Rock Mech Min Sci 88:307–317

Jiang LS, Wang P, Zhang PP, Zheng PQ, Xu B (2017) Numerical analysis of the effects induced by normal faults and dip angles on rock bursts. C R Mec 345(10):690–705

Jiang JQ, Wang P, Jiang LS, Zheng PQ, Feng F (2018) Numerical simulation on mining effect influenced by a normal fault and its induced effect on rock burst. Geomech Eng 14(4):337–344

Jiang LS, Kong P, Shu JM, Fan KG (2019a) Numerical analysis of support designs based on a case study of a longwall entry. Rock Mech Rock Eng. https://doi.org/10.1007/s00603-018-1728-2

Jiang LS, Wang P, Zheng PQ, Luan HJ, Zhang C (2019b) Influence of different advancing directions on mining effect caused by a fault. Adv Civil Eng 2019:7306850

Li T, Mu ZL, Liu GJ, Du JL, Lu H (2016) Stress spatial evolution law and rockburst danger induced by coal mining in fault zone. Int J Min Sci Technol 26(3):409–415

Liu CY, Yetilmezsoy K, Zhang BS, Zhang S (2017) Fractural structure of thick hard roof stratum using long beam theory and numerical modeling. Environ Earth Sci 76(21):751

Lv JG, Jiang YD, Li SG, Ren SD, Jiang WZ, Zhang ZC (2014) Characteristic and mechanism research of coal bumps induced by faults based on extra thick and hard roof. J China Coal Soc 39(10):1961–1969

Ning JG, Wang J, Jiang LS, Jiang N, Liu XS, Jiang JQ (2017) Fracture analysis of double-layer hard and thick roof and the controlling effect on strata behavior: a case study. Eng Fail Anal 81:117–134

Qi QX, Dou LM (2008) Theory and technology of rockburst. China University of Mining and Technology press, Xuzhou, p 3

Rutqvist J, Rinaldi AP, Cappa F, Moridis GJ (2015) Modeling of fault activation and seismicity by injection directly into a fault zone associated with hydraulic fracturing of shale-gas reservoirs. J Petrol Sci Eng 127:377–386

Sainoki A, Mitri HS (2014a) Dynamic behaviour of mining-induced fault slip. Int J Rock Mech Min Sci 66C(1):19–29

Sainoki A, Mitri HS (2014b) Dynamic modelling of fault-slip with Barton's shear strength model. Int J Rock Mech Min Sci 67(6):155–163

Sainoki A, Mitri HS (2014c) Methodology for the interpretation of fault-slip seismicity in a weak shear zone. J Appl Geophys 110:126–134

Sainoki A, Mitri HS (2015a) Influence of undulating fault surface properties on its seismic waves during fault-slip. Int J Min Reclam Environ 30(1):1–12

Sainoki A, Mitri HS (2015b) Evaluation of fault-slip potential due to shearing of fault asperities. Can Geotech J 52:1417–1425

Wang L, Cheng YP, Xu C, An FH, Jin K, Zhang XL (2013) The controlling effect of t hick-hard igneous rock on pressure relief gas drainage and dynamic disasters in outburst coal seams. Nat Hazards 66(2):1221–1241

Wang W, Cheng YP, Wang HF, Liu HY, Wang L, Li W, Jiang JY (2015) Fracture failure analysis of hard-thick sandstone roof and its controlling effect on gas emission in underground ultrathick coal extraction. Eng Fail Anal 54:150–162

Wang P, Jiang JQ, Zhang PP, Wu QL (2016) Breaking process and mining stress evolution characteristics of a high-position hard and thick stratum. Int J Min Sci Technol 26(4):563–569

Wang P, Jiang LS, Zheng PQ (2017) Application of equivalent materials to modeling fractures in the vicinity of a normal fault in the area of mining exploitation influence. Acta Geodynamica et Geomaterialia 14(4):475–485

Wang P, Jiang LS, Jiang JQ, Zheng PQ, Li W (2018a) Strata behaviors and rock burst–inducing mechanism under the coupling effect of a hard, thick stratum and a normal fault. Int J Geomech 18(2):04017135. https://doi.org/10.1061/(asce)gm.1943-5622.0001044

Wang P, Jiang LS, Li XY, Zheng PQ, Qin GP (2018b) Effects of strength weakening and interface slipping on rock mass with different dip angle structure planes. Acta Geodynamica et Geomaterialia 15(4):329–338

Wang P, Jiang LS, Li XY, Qin GP, Wang EY (2018c) Physical simulation of mining effect caused by a fault tectonic. Arab J Geosci 11(23):741. https://doi.org/10.1007/s12517-018-4088-z

Xia BW, Jia JL, Yu B, Zhang X, Li XL (2017) Coupling effects of coal pillars of thick coal seams in large-space stopes and hard stratum on mine pressure. Int J Min Sci Technol 27(6):965–972

Xu NW, Tang CA, Li LC, Zhou Z, Sha C, Liang ZZ, Yang JY (2011) Microseismic monitoring and stability analysis of the left bank slope in Jinping first stage hydropower station in southwestern China. Int J Rock Mech Min Sci 48(6):950–963

Zhao X, Lv JG (2015) Mechanical analysis of coal and rock dynamic instability by thick and hard roof thrust fault. Saf Coal Mines 46(1):198–201 **(Chinese)**

Zhou H, Meng FZ, Zhang CQ, Hu DW, Yang FJ, Lu JJ (2015) Analysis of rockburst mechanisms induced by structural planes in deep tunnels. Bull Eng Geol Env 74(4):1–17